Preparation of Mg(OH)2 nanoparticles modified PVDF membranes for efficient dye adsorption and rejection

Ying Cai[a,b], Jian Lu[a,b], Jun Wu[c,*]

[a]*CAS Key Laboratory of Coastal Environmental Processes and Ecological Remediation, Yantai Institute of Coastal Zone Research (YIC), Chinese Academy of Sciences (CAS), Yantai, Shandong 264003, China*
[b]*Shandong Key Laboratory of Coastal Environmental Processes, Yantai Institute of Coastal Zone Research (YIC), Chinese Academy of Sciences (CAS), Yantai, Shandong 264003, China*
[c]*Yantai Research Institute and Graduate School, Harbin Engineering University, Yantai, Shandong 265501, China, email: wujunlisa@163.com (J. Wu)*

ABSTRACT

$Mg(OH)_2$ nanoparticles were successfully prepared and incorporated in the poly(vinylidene fluoride) (PVDF) membranes to enhance the hydrophilicity, anti-fouling, and dye treatment capacity. The products were characterized by multiple techniques including scanning electron microscopy, size distribution by intensity, Fourier transform infrared, powder X-ray diffraction, the Brunauer–Emmett–Teller surface area, and energy dispersive spectrometer elemental mapping. $Mg(OH)_2$ nanoparticles possessed uniform particle sizes and were homogeneously dispersed in the PVDF matrix with less aggregation. The incorporation of $Mg(OH)_2$ nanoparticles into PVDF composite membranes caused a decrease in the contact angle and great improvements in the pure water flux from 252 to 471 L m^{-2} h^{-1} and bovine serum albumin rejection from 40% to 80% at the same time. In addition, the composite membranes had a significant increase in adsorption of cationic dyes methylene blue from 4.6 to 8.3 μg cm^{-2} and rejection from 11% to 21% when $Mg(OH)_2$ nanoparticles were added from 0 to 1.5 wt.% due to the good adsorption for dyes of $Mg(OH)_2$ nanoparticles. The removal rate of anionic dye Congo red increased from 72% to 98% and rejection increased from 13% to 80% when $Mg(OH)_2$ nanoparticles were added from 0 to 1.5 wt.%. This study provides information on application potential of $Mg(OH)_2$ nanoparticles incorporated in membranes for treating dye wastewater.

Keywords: Polyvinylidene fluoride composite membranes; $Mg(OH)_2$ nanoparticles; Anti-fouling; Dye absorption and rejection

1. Introduction

In recent years, the use of organic dyes has increased rapidly with the rapid development of printing and dyeing industry. These organic compounds with a complex aromatic molecular structure are non-degradable and toxic, even in the presence of very small amounts of organic compounds in water [1–4]. Therefore, a series of technologies have been developed including biological processes [5], biochemical processes [6], chemical oxidation [7], adsorption [8,9], coagulation [10,11], and membrane [12,13] treatments to remove dyes from wastewater [14,15]. Among these methods, physical adsorption is thought to be an effective and economical method because of its high efficiency in removing dyes and easy access in gaining the adsorbents [16]. Many articles reported the adsorption of dyes on different adsorbents such as activated carbon [17], silica [18], clay [9], polymers [19,20], alumina [21], $Mg(OH)_2$ [22], and so on.

$Mg(OH)_2$ has attracted wide attention due to its low cost, antibacterial, non-toxic, good thermal stability, and

---

* Corresponding author.

other characteristics as a green treatment agent [23,24]. Wastewater treatment is one of the most widely used applications of $Mg(OH)_2$. $Mg(OH)_2$ usually has a hexagonal symmetry structure, which exhibits plate-like morphology with a large specific surface area [25]. The adsorption capacity of $Mg(OH)_2$ mainly depends on its surface area [23]. The smaller size of $Mg(OH)_2$ nanoparticles, the lager Brunauer–Emmett–Teller (BET) surface area and the higher adsorption rate during the reaction [26]. Therefore, $Mg(OH)_2$ nanoparticles may be a good candidate for dye wastewater treatment. In addition, $Mg(OH)_2$ nanoparticles also exhibit high selective adsorption capacity and fast adsorption rate for the removal of anionic dye. The adsorbed dye can be successfully desorbed by carbonation, resulting in a 4,000 times enrichment of the dye solution [27].
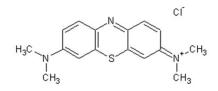
Membrane technology is one of the effective methods to remove dyes from wastewater [3]. Membrane-based wastewater purification technologies are considered to be feasible and cost-effective [4]. The addition of inorganic fillers into the membrane can improve performance and play a better role in the water treatment process. At the same time, the interaction between the membrane material and the filler also has a certain impact on the performance of the membrane [28–31]. $Mg(OH)_2$ is one of better choice in the numerous inorganic fillers.

$Mg(OH)_2$ with structurally bound hydroxyls is used more and more frequently in the production of multifunctional membranes[32]. Dong et al. [32] used $Mg(OH)_2$ as a component in the production of an organic–inorganic composite membrane together with poly(vinylidene fluoride) (PVDF) based on a reversed phase inversion method. The properties of the membrane were also modified with the use of poly(ethylene glycol). $Mg(OH)_2$ is also used as an effective agent against the bacteria *Escherichia coli* and *Burkholderia phytofirmans* [33]. This study will report the application potential of $Mg(OH)_2$ nanoparticles that were used to improve hydrophilicity, anti-fouling performance, and dye wastewater treatment capacity of PVDF composite membranes.
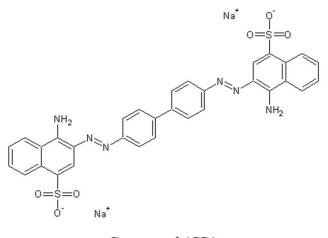
2. Materials and methods

2.1. Materials and reagents

PVDF (Mn = 110,000 g mol^{-1}, Solef 6010) was purchased from Solvay Solexis (Belgium). PVDF was vacuum drying at 110°C for 24 h before use. DMAc (analytical reagent grade), polyvinylpyrrolidone (PVP K30), $MgCl_2 \cdot 6H_2O$ (magnesium chloride hexahydrate), polyethylene glycol (PEG 400) and $NH_3 \cdot H_2O$ were obtained from Sinopharm Chemical Reagent Co., (Beijing, China) and used without further purification in this experiment. Bovine serum albumin (BSA, with molecular weight of 67,000 Da) obtained from Sigma-Aldrich Co., (St. Louis, USA) was used as received. Phosphate buffer solution (PBS pH = 7.2–7.4) was obtained from Beijing Solarbio Science and Technology Co., (Beijing, China). *Escherichia coli* ATCC 25922 (*E. coli*) strains were used in this study. The cationic dye Methylene blue (MB, $C_{16}H_{18}ClN_3S$, M_w = 319.86 Da) and the anionic dyes Congo red (CR, $C_{32}H_{22}N_6Na_2O_6S_2$, M_w = 696.68 Da) were purchased from Tianjin Hengxing Chemical Reagent Co., (China) and their structures were show in Fig. 1.

Fig. 1. Chemical structures of cationic dye Methylene blue (MB) and anionic dye Congo red (CR).

2.2. Preparation of Mg(OH)₂ nanoparticles

The typical procedure for the preparation of $Mg(OH)_2$ nanoparticles was as the following: 1 mol $MgCl_2 \cdot 6H_2O$ and 20 mL PEG 400 were dissolved in 200 mL deionized water to form a transparent solution. With constant magnetic stirring at 50°C for 1 h, 16 mL $NH_3 \cdot H_2O$ was added dropwisely to the above solution through a dropping funnel. The resulting mixture was kept at that temperature for 4 h, and then held at room temperature for another 1.5 h. The nanoparticles were collected by filtration and washed with deionized water and ethanol several times, respectively, to remove the ions possibly remaining in the final product. Finally, the products were dried overnight at 60°C under vacuum [34].

2.3. Preparation of PVDF composite membranes

PVDF membranes were prepared by nonsolvent-induced phase separation (NIPS) method. $Mg(OH)_2$ nanoparticles and PVP powders were ultrasonically dispersed in DMAc for 1 h and then agitated for 24 h before adding PVDF. The casting solution was mechanically stirred at 40°C until the polymer was completed dissolved. Then the casting solution was left at vacuum dryer for 24 h for the sake of removing air bubbles. The casting solution was casted onto a glass plate using a casing knife with the casting thickness of about 200 μm. The glass plate was then put into the water bath immediately to form a PVDF membrane at room temperature. The compositions of these PVDF membranes were exhibited in Table 1.

Table 1
Detailed composition of different membranes

Type of membrane	PVDF (wt.%)	Mg(OH)$_2$ (wt.%)	PVP (wt.%)	DMAc (wt.%)
M0	18	0	2	80
M1	18	0.5	2	79.5
M2	18	1	2	79
M3	18	1.5	2	78.5
M4	18	2	2	78
M5	18	3	2	77

2.4. Characterization of Mg(OH)$_2$ nanoparticles and PVDF membranes

The structure of Mg(OH)$_2$ nanoparticles and the membranes including top surface (water side) and cross section were measured by a field emission scanning electron microscopy (FESEM) (Hitachi S-4800, Hitachi Ltd., Japan). The cross-section images of PVDF membranes were acquired after being freeze-dried and fractured in liquid nitrogen. Moreover, elemental mapping of silicon and aluminum in the PVDF composite membranes were obtained using an energy dispersive spectrometer (EDS) (Hitachi S-4800, Hitachi Ltd., Japan). The size distribution of the Mg(OH)$_2$ nanoparticles was carried out using a dynamic light scattering measurements with Zetasizer Nano ZS (Malvern Instruments, Malvern, UK). The BET surface area of the Mg(OH)$_2$ nanoparticles was studied using a nitrogen adsorption instrument (Micromeritics ASAP 2460, Norcross, GA, USA). All samples were degassed at 200°C for 1 h prior to actual measurements. The Fourier transform infrared (FTIR) spectra of Mg(OH)$_2$ nanoparticles and PVDF membranes were tested by a JASCO 4100 instrument (JASCO, Japan) at room temperature from 500 to 4,000 cm^{-1}. The pH at the point of zero charge (pHzc) of the catalyst was determined by testing the zeta potential at different pH conditions using a Zetasizer Nano S (Malvern Instruments, Malvern, UK).

The water contact angle (CA) was measured to studies the surface hydrophobicity of the PVDF membranes. A contact angle analyzer (OCA50, Dataphysics, Germany) was used in this measurement. Approximately 2 μL of DI water droplets were dropped onto the top surface of PVDF membrane samples at ambient temperature. Experimental data were acquired at least five times at different sites of each PVDF membrane. The filtration performance was conducted using a typically lab-scale cross-flow filtration system. The system has an effective surface area of 8 cm². In each test, PVDF membrane samples were tested at 0.15 Mpa using DI water for 30 min before measurements were taken at 0.1 Mpa and 25°C for 30 min. The pure water flux (PWF) was computed according to the below equation:

$$J_w = \frac{Q}{A \cdot \Delta T} \tag{1}$$

where J_w is the pure water flux (PWF, Lm^{-2}h^{-1}), Q is volume of the permeated pure water (L), A is the effective filtration membrane area (m²), and ΔT is the permeation time (h).

BSA rejection of the PVDF membrane was tested at 0.1 MPa and 25°C. BSA with concentration of 1 g L^{-1} was dissolved in PBS solution (pH 7.4). BSA rejection (R) was calculated as Eq. (2).

$$R(\%) = \left(1 - \frac{C_p}{C_0}\right) \times 100 \tag{2}$$

where C_p and C_0 are the concentration of protein in the permeation and the feed solution, respectively. The BSA concentrations in the permeation and the feed solution were evaluated using a Puxi TU-1810 scanning spectrophotometer (Puxi Analytic Instrument Ltd., Beijing, China) at wavelength of 280 nm.

The membrane samples were immersed into *E. coli*-containing Luria–Bertani (LB) media at room temperature for 24 h. Membranes were taken from bacterial suspension and gently washed with PBS. The mild ultrasonication was used for 10 min in order to dislodge the bacteria adhering to the membrane surfaces, but to retain the adsorbed ones. The membranes were then immersed in 3 vol.% glutaraldehyde in PBS for 4 h, and then dehydrated for 10 min with 50%, 70%, 90%, and 100% ethanol in turn for the bacterial fixation [35]. The membranes obtained were observed by SEM.

2.5. Dye adsorption and rejection experiments

The adsorption measurement of PVDF membranes was carried out using the immersing method with cation MB and anion CR. The dyes were firstly dissolved in distilled water to form a homogeneous solution with the concentration of 20 ppm. Then, PVDF membranes with the same surface area (10 cm²) were cut into small pieces and were separately immersed in the dye aqueous solutions (15 mL) for 24 times at room temperature. The PVDF membranes were then taken out and the residual amount of MB and CR in the aqueous solution was detected using a TU-1810 spectrophotometer (Puxi Analytic Instrument Ltd., Beijing, China) at the wavelength of 664 and 497 nm separately [36]. The dye removal was determined by the below Eq. (3).

$$D(\%) = \left(1 - \frac{D_e}{D_0}\right) \times 10 \tag{3}$$

where D_e and D_0 are final and initial the concentration of dye for the adsorption experiment, respectively.

Dye flux and rejection of the PVDF membrane was tested at 0.1 MPa and 25°C. MB and CR solutions with concentrations of 20 ppm were used as feed. Dye flux was calculated as Eq. (1). Dye rejection (*R*) was calculated as Eq. (2).

3. Results and discussion

3.1. Characterization of Mg(OH)₂ nanoparticles

Fig. 2A shows the scanning electron microscopy (SEM) image of $Mg(OH)_2$ nanoparticles which had a uniform lamellar structure average size of about 300 nm × 300 nm × 20 nm. Fig. 2B shows the particle size distribution curve of $Mg(OH)_2$ nanoparticles which had a narrow size distribution with particles size around 280 nm to be beneficial for the uniform distribution of the particles. The BET surface area of $Mg(OH)_2$ nanoparticles was 42.93 m^2 g^{-1}. The pH_{ZC} of the synthesized nano-$Mg(OH)_2$ in this study was 6.7.

3.2. Characterization of PVDF membranes

The FTIR curves of $Mg(OH)_2$ nanoparticles, called *M0* and *M3*, are shown in Fig. 3. The FTIR spectrum of the $Mg(OH)_2$ nanoparticles showed the characteristic peaks which were similar to those reported in the literature [37,38]. The sharp peak at 3,698 cm^{-1} was attributed to the
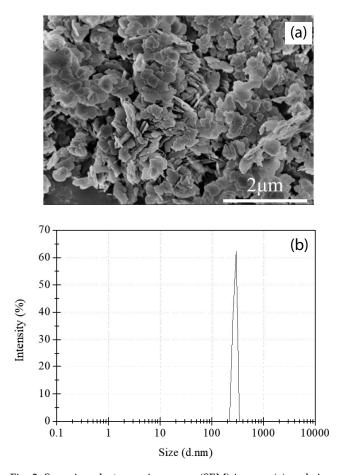
stretching vibration of OH group in $Mg(OH)_2$ while the flat peak at 3,440 cm^{-1} belonged to the adsorbed water [39]. Bands in the range of 1,636–1,425 cm^{-1} were the result of the stretching vibration mode of OH group in water [40]. The characteristic peaks of pure membrane (*M0*) at 3,023 and 2,982 cm^{-1} were resulted from the asymmetrical CH stretching and symmetrical CH stretching [41]. The peaks at 1,403–1,067 cm^{-1} corresponded to the deformation vibration of CF of PVDF [42,43]. Apparently, both two peaks 3,698 and 3,440 cm^{-1} appeared with the incorporation of $Mg(OH)_2$ nanoparticles (*M3*). These results suggested that $Mg(OH)_2$ nanoparticles were successfully blended with PVDF.

SEM images of the top and bottom surface and cross-section of the PVDF membranes are shown in Fig. 4. All membranes exhibited an asymmetrical structure with a dense skin layer and a porous bottom surface [43]. For the pristine PVDF membrane (*M0*), the DMAc in the outer surface rapidly exchanged with water to result in the unstable thermodynamic system in the top surface to form a uniform and dense top surface instantly (M0T) when the casting solution immersed in water [36]. The hydrophilicity $Mg(OH)_2$ nanoparticles were uniformly dispersed in the modified membranes to make wrinkles increase on the top surface and roughness increase. Meanwhile the number of pores and pore size on the bottom surface increased with the addition of $Mg(OH)_2$ nanoparticles [32]. The incorporation of $Mg(OH)_2$ nanoparticles in membrane casting solution caused larger pore size and higher surface porosity due to the pore-forming effect of $Mg(OH)_2$ nanoparticles [44].

It can be seen that the number of pores on the membrane surface increased with the addition of $Mg(OH)_2$ nanoparticles. It is assumed that the $Mg(OH)_2$ nanoparticles are dispersed uniformly in the casting suspension. The hydrophilic nanoparticles have a high tendency to adsorb water during phase inversion, which contributes to more sites for water penetration and more pores formed on the skin layer of the membrane. The structure of cross-section has not changed much with the addition of $Mg(OH)_2$ nanoparticles.
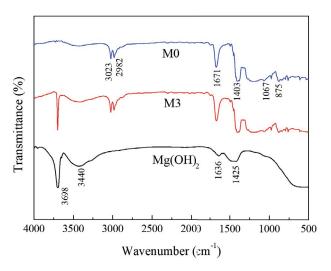

Fig. 2. Scanning electron microscopy (SEM) images (a) and size distribution by intensity (b) of $Mg(OH)_2$ nanoparticles.

Fig. 3. Fourier transform infrared (FTIR) curves of $Mg(OH)_2$ nanoparticles, *M0* and *M3*.

Fig. 4. SEM images of top surface (*T*), bottom surface (*B*), and cross-sections (*S*) of PVDF composite membranes (*M*0–*M*5).

Fig. 5 shows the EDX mapping image for elements Mg, C, F, and O on top surface of the PVDF composite membrane (*M*3). The dispersion of Mg was relatively uniform, which indicated that $Mg(OH)_2$ nanoparticles were dispersible uniformity on the surface of composite membrane without obvious aggregation.

3.3. Membrane permeation and anti-fouling characteristics

Fig. 6 shows the water contact angle, pure water flux, and BSA rejection of the PVDF membranes. The pristine PVDF membrane (*M*0) was hydrophobic, and the water contact angle was about 70° (Fig. 6A). A large number of hydrophilic groups –OH appeared on the membrane surface as the incorporation of the $Mg(OH)_2$ nanoparticles to result in an increase in the hydrophilicity on the membrane top surface, and decrease in the water contact angle of the composite membranes (*M*3). The excessive $Mg(OH)_2$ nanoparticles will produce agglomeration phenomenon when the concentration

of $Mg(OH)_2$ nanoparticles continues to increase. Therefore, the hydrophilicity of the surface was not further improved (*M*4–*M*5).

The water contact angle test corresponded to the results of the pure water flux and retention of the membranes (Fig. 6B). The pure water flux and the BSA retention rate of the pristine PVDF membrane were 252 L m^{-2} h^{-1} and 40%, respectively. The PWF of the composite membrane was significantly enhanced by a small amount of $Mg(OH)_2$ NPs addition. The PWF raised to 471 L m^{-2} h^{-1} when the NPs increased to 1.5 wt.%. This might be caused by that the addition of appropriate amount of $Mg(OH)_2$ NPs under the condition of keeping the PVDF concentration constant reduced the number of PVDF molecules per unit volume, weakened the intermolecular force of polymer, and made the structure of the prepared membrane relatively loose and the water molecules easy to pass through. In addition, the hydrophilicity of $Mg(OH)_2$ NPs also improved the pure water flux. For the rejection of the membranes, the BSA
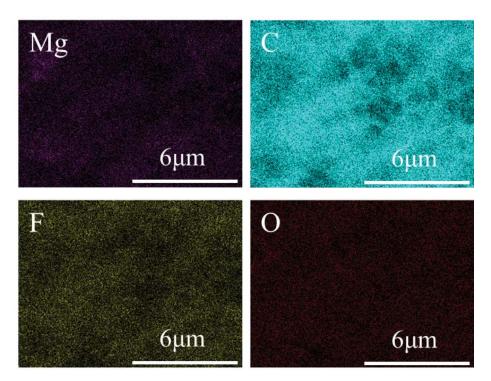
Fig. 5. Energy dispersive spectrometer (EDS) elemental mapping of Mg, C, F, and O on the top surface of PVDF composite membranes (M3).
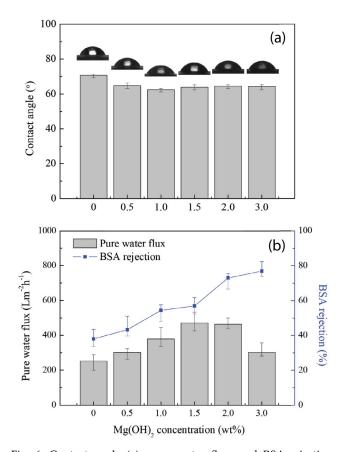

Fig. 6. Contact angle (a), pure water flux, and BSA rejection (b) of PVDF composite membranes with different Mg(OH)$_2$ concentration.

rejection increased significantly with the increase of the Mg(OH)$_2$ nanoparticles. This might be ascribed to that the surface of nano-Mg(OH)$_2$ anionized through the deprotonation process when the solution pH was greater than its pH$_{ZC}$ (6.7) under neutral or alkaline conditions while the BSA was also anionized under the same conditions. The nano Mg(OH)$_2$ NPs had the rejection effect on BSA to subsequently improve the retention of BSA by the membrane. The viscosity of the casting solution would increase sharply as the concentration of Mg(OH)$_2$ continued to increase, which reduced the double diffusion speed of water and solvent in the process of membrane formation. The membrane structure was relatively tight to hinder the passage of water molecules, resulting in a significant decrease in water flux (M4–M5). At this time, the rejection rate of membrane continued to increase. As the addition amount of nanoparticles reached 3.0wt.%, the rejection rate increased to 80%. Additionally, the Mg(OH)$_2$ nanoparticles inhibited the biofilm formation on the membrane surface and the antifouling properties were thereby enhanced [32,45].

3.4. Dye adsorption and rejection

Figs. 7 and 8 show adsorption as well as flux and rejection of membranes of the cationic MB and anionic CR, respectively. The MB adsorption was almost doubled from 4.6 to 8.3 µg cm^{-2} when the Mg(OH)$_2$ nanoparticle concentrations increased from 0 to 1.5 wt.% (Fig. 7B). It could also be seen in the photo that the membranes M3 was bluer than M0 in Fig. 7A. The adsorption capacity of MB decreased as the content of Mg(OH)$_2$ nanoparticles continuously increased, which might be ascribed to the agglomeration of a large number of Mg(OH)$_2$ nanoparticles to reduce the adsorption
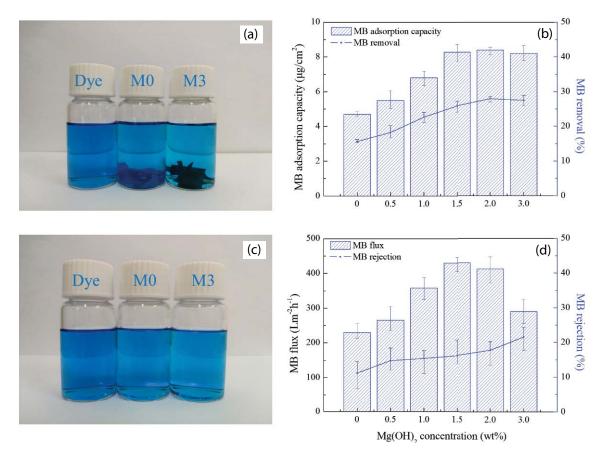
Fig. 7. MB adsorption capacity and removal (a and b), MB flux, and rejection (c and d) of PVDF composite membranes with different Mg(OH)$_2$ concentration.

capacity. The addition of magnesium hydroxide made the rejection of MB increase from 11% to 21% (Fig. 7D). The CR adsorption capacity increased from 20 to 28 μg cm^{-2} and the final removal rate of CR reached 98% as the Mg(OH)$_2$ nanoparticle concentrations increased from 0 to 1.5 wt.%. The CR rejection of the pristine PVDF membrane was only 13% while the rejection increased to around 80% as the incorporation of the Mg(OH)$_2$ nanoparticles (Fig. 8). Since the surface of nano-Mg(OH)$_2$ was anionized through the deprotonation process when the solution pH is greater than its pH$_{ZC}$ (6.7) under neutral or alkaline conditions, the rejection of the anionic dyes was sharply enhanced using the nano-Mg(OH)$_2$ modified PVDF membrane. A large number of magnesium hydroxide in PVDF unevenly dispersed due to the poor compatibility of polymer PVDF and inorganic magnesium hydroxide when the content of magnesium hydroxide in the membrane continued to increase (2.0%–3.0%), which made nano-Mg(OH)$_2$ agglomerate to reduce the adsorption efficiency of the membrane materials for dyes. In addition, high-concentration magnesium hydroxide would increase the viscosity of the casting solution, reduce the mass transfer rate in the process of membrane formation, and easily form a relatively compact membrane structure, resulting in the decrease of dye flux and the increase of dye retention (Figs. 7D and 8D). The results show that appropriate Mg(OH)$_2$ nanoparticles are beneficial to the dye absorption and rejection especially for the anionic dyes (CR).

4. Conclusions

High performance PVDF composite membrane were prepared successfully via blending with laboratory-prepared Mg(OH)$_2$ nanoparticles. The characterizations of FTIR, XRD, SEM, and EDS elemental mapping indicated that Mg(OH)$_2$ nanoparticles were well dispersed in PVDF composite membranes. The incorporation of Mg(OH)$_2$ nanoparticles promoted the hydrophilicity and PWF of the PVDF membranes because of the hydrophilicity of Mg(OH)$_2$ nanoparticles. Moreover, adsorption and rejection of dyes by modified membranes increased dramatically. This work provides a new insight on the use of Mg(OH)$_2$ nanoparticles for modification of PVDF membrane, which might broaden the technologies for water treatment.
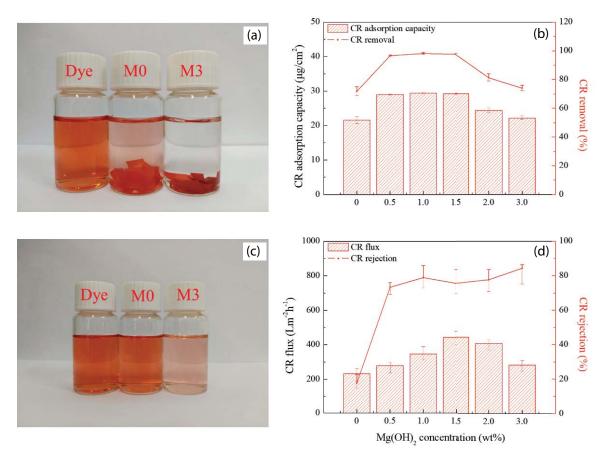
Fig. 8. CR adsorption capacity and removal (A and B), CR flux, and rejection (C and D) of PVDF composite membranes with different Mg(OH)$_2$ concentration.

References

[1] A.J. Kajekar, B.M. Dodamani, A.M. Isloor, Z.A. Karim, N.B. Cheer, A.F. Ismail, S.J. Shilton, Preparation and characterization of novel PSf/PVP/PANI-nanofiber nanocomposite hollow fiber ultrafiltration membranes and their possible applications for hazardous dye rejection, Desalination, 365 (2015) 117–125.

[2] A. Aouni, C. Fersi, B. Cuartas-Uribe, A. Bes-Pía, M.I. Alcaina-Miranda, M. Dhahbi, Reactive dyes rejection and textile effluent treatment study using ultrafiltration and nanofiltration processes, Desalination, 297 (2012) 87–96.

[3] N. Nikooe, E. Saljoughi, Preparation and characterization of novel PVDF nanofiltration membranes with hydrophilic property for filtration of dye aqueous solution, Appl. Surf. Sci., 413 (2017) 41–49.

[4] S. Foorginezhad, M.M. Zerafat, Microfiltration of cationic dyes using nano-clay membranes, Ceram. Int., 43 (2017) 15146–15159.

[5] A. Paz, J. Carballo, M.J. Pérez, J.M. Domínguez, Biological treatment of model dyes and textile wastewaters, Chemosphere, 181 (2017) 168–177.

[6] M.A. Rauf, S. Salman Ashraf, Survey of recent trends in biochemically assisted degradation of dyes, Chem. Eng. J., 209 (2012) 520–530.

[7] A.A. Azzaz, S. Jellali, H. Akrout, A.A. Assadi, L. Bousselmi, Dynamic investigations on cationic dye desorption from chemically modified lignocellulosic material using a low-cost eluent: dye recovery and anodic oxidation efficiencies of the desorbed solutions, J. Cleaner Prod., 201 (2018) 28–38.

[8] R.-Z. Zhang, S. Quan, M. Xia, Q. Wang, W. Zhang, J.-M. Yang, Effect of surface charge status of amorphous porous coordination polymer particles on the adsorption of organic dyes from an aqueous solution, J. Colloid Interface Sci., 525 (2018) 54–61.

[9] A. Kausar, M. Iqbal, A. Javed, K. Aftab, Z.i.H. Nazli, H.N. Bhatti, S. Nouren, Dyes adsorption using clay and modified clay: a review, J. Mol. Liq., 256 (2018) 395–407.

[10] A. Ozkan, M. Yekeler, Coagulation and flocculation characteristics of celestite with different inorganic salts and polymers, Chem. Eng. Process. Process Intensif., 43 (2004) 873–879.

[11] B.-Y. Gao, Q.-Y. Yue, Y. Wang, W.-Z. Zhou, Color removal from dye-containing wastewater by magnesium chloride, J. Environ. Manage., 82 (2007) 167–172.

[12] H.-M. Xu, X.-F. Sun, S.-Y. Wang, C. Song, S.-G. Wang, Development of laccase/graphene oxide membrane for enhanced synthetic dyes separation and degradation, Sep. Purif. Technol., 204 (2018) 255–260.

[13] M. Liu, Q. Chen, K. Lu, W. Huang, Z. Lü, C. Zhou, S. Yu, C. Gao, High efficient removal of dyes from aqueous solution through nanofiltration using diethanolamine-modified polyamide thin-film composite membrane, Sep. Purif. Technol., 173 (2017) 135–143.

[14] S.R. Kavitha, M. Umadevi, S.R. Janani, T. Balakrishnan, R. Ramanibai, Fluorescence quenching and photocatalytic degradation of textile dyeing waste water by silver nanoparticles, Spectrochim. Acta, Part A, 127 (2014) 115–121.

[15] J.-Z. Lian, C.-T. Tsai, S.-H. Chang, N.-H. Lin, Y.-H. Hsieh, Iron waste as an effective depend on TiO$_2$ for photocatalytic degradation of dye waste water, Optik, 140 (2017) 197–204.

[16] M. Liu, J. Xu, B. Cheng, W. Ho, J. Yu, Synthesis and adsorption performance of Mg(OH)$_2$ hexagonal nanosheet–graphene oxide composites, Appl. Surf. Sci., 332 (2015) 121–129.

[17] R.K. Liew, E. Azwar, P.N.Y. Yek, X.Y. Lim, C.K. Cheng, J.-H. Ng, A. Jusoh, W.H. Lam, M.D. Ibrahim, N.L. Ma, S.S. Lam, Microwave pyrolysis with KOH/NaOH mixture activation: a new approach to produce micro-mesoporous activated carbon for textile dye adsorption, Bioresour. Technol., 266 (2018) 1–10.

[18] S.O. Akpotu, B. Moodley, Effect of synthesis conditions on the morphology of mesoporous silica from elephant grass and its application in the adsorption of cationic and anionic dyes, J. Environ. Chem. Eng., 6 (2018) 5341–5350.

[19] D. Das, C.K. Karan, M. Bhattacharjee, Heterotrimetallic coordination polymers for dye adsorption and desorption, Polyhedron, 124 (2017) 51–61.

[20] X. Li, M. Zhou, J. Jia, Q. Jia, A water-insoluble viologen-based β-cyclodextrin polymer for selective adsorption toward anionic dyes, React. Funct. Polym., 126 (2018) 20–26.

[21] B. Yahyaei, S. Azizian, Rapid adsorption of binary dye pollutants onto the nanostructred mesoporous alumina, J. Mol. Liq., 199 (2014) 88–95.

[22] M. Shamsayei, Y. Yamini, H. Asiabi, Fabrication of zwitterionic histidine/layered double hydroxide hybrid nanosheets for highly efficient and fast removal of anionic dyes, J. Colloid Interface Sci., 529 (2018) 255–264.

[23] A.A. Pilarska, Ł. Klapiszewski, T. Jesionowski, Recent development in the synthesis, modification and application of $Mg(OH)_2$ and MgO: a review, Powder Technol., 319 (2017) 373–407.

[24] A. Pilarska, K. Bula, K. Myszka, T. Rozmanowski, K. Szwarc-Rzepka, K. Pilarski, L. Chrzanowski, K. Czaczyk, T. Jesionowski, Functional polypropylene composites filled with ultra-fine magnesium hydroxide, Open Chem., 13 (2015) 161–171.

[25] P.P. Wang, Y.X. Ye, D.W. Liang, H.M. Sun, J. Liu, Z.F. Tian, C.H. Liang, Layered mesoporous $Mg(OH)_2$/GO nanosheet composite for efficient removal of water contaminants, RSC Adv., 6 (2016) 26977–26983.

[26] C.R. Li, Z.Y. Zhuang, F. Huang, Z.C. Wu, Y.P. Hong, Z.Lin, Recycling rare earth elements from industrial wastewater with flowerlike nano-$Mg(OH)_2$, ACS Appl. Mater. Interfaces, 5 (2013) 9719–9725.

[27] Y.J. Wang, J.P. Chen, L.L. Lu, Z. Lin, Reversible switch between bulk $MgCO_3$·$3H_2O$ and $Mg(OH)_2$ micro/nanorods induces continuous selective preconcentration of anionic dyes, ACS Appl. Mater. Interfaces, 5 (2013) 7698–7703.

[28] D. Rana, K. Bag, S.N. Bhattacharyya, B.M. Mandal, Miscibility of poly(styrene-*co*-butyl acrylate) with poly(ethyl methacrylate): existence of both UCST and LCST, J. Polym. Sci., Part B: Polym. Phys., 38 (2000) 369–375.

[29] D. Rana, B.M. Mandal, S.N. Bhattacharyya, Analogue calorimetric studies of blends of poly(vinyl ester)s and polyacrylates, Macromolecules, 29 (1996) 1579–1583.

[30] D. Rana, B.M. Mandal, S.N. Bhattacharyya, Analogue calorimetry of polymer blends: poly(styrene-*co*-acrylonitrile) and poly(phenyl acrylate) or poly(vinyl benzoate), Polymer, 37 (1996) 2439–2443.

[31] D. Rana, B.M. Mandal, S.N. Bhattacharyya, Miscibility and phase-diagrams of poly(phenyl acrylate) and poly(styrene-*co*-acrylonitrile) blends, Polymer, 34 (1993) 1454–1459.

[32] C. Dong, G. He, H. Li, R. Zhao, Y. Han, Y. Deng, Antifouling enhancement of poly(vinylidene fluoride) microfiltration membrane by adding $Mg(OH)_2$ nanoparticles, J. Membr. Sci., 387–388 (2012) 40–47.

[33] C.X. Dong, J. Cairney, Q.H. Sun, O.L. Maddan, G.H. He, Y.L. Deng, Investigation of $Mg(OH)_2$ nanoparticles as an antibacterial agent, J. Nanopart. Res., 12 (2010) 2101–2109.

[34] W. Wang, X. Qiao, J. Chen, H. Li, Facile synthesis of magnesium oxide nanoplates via chemical precipitation, Mater. Lett., 61 (2007) 3218–3220.

[35] C. Yao, X. Li, K.G. Neoh, Z. Shi, E.T. Kang, Surface modification and antibacterial activity of electrospun polyurethane fibrous membranes with quaternary ammonium moieties, J. Membr. Sci., 320 (2008) 259–267.

[36] Z. Zhu, L. Wang, Y. Xu, Q. Li, J. Jiang, X. Wang, Preparation and characteristics of graphene oxide-blending PVDF nanohybrid membranes and their applications for hazardous dye adsorption and rejection, J. Colloid Interface Sci., 504 (2017) 429–439.

[37] J.-P. Hsu, A. Nacu, Preparation of submicron-sized $Mg(OH)_2$ particles through precipitation, Colloids Surf., A, 262 (2005) 220–231.

[38] S. Yousefi, B. Ghasemi, M. Tajally, A. Asghari, Optical properties of MgO and $Mg(OH)_2$ nanostructures synthesized by a chemical precipitation method using impure brine, J. Alloys Compd., 711 (2017) 521–529.

[39] S.Y. Wang, G.M. Li, W. Xu, C. Liu, L. Dai, H.C. Zhu, Facile preparation and application of magnesium hydroxide assembly spheres, Res. Chem. Intermed., 42 (2016) 2661–2668.

[40] D. An, X. Ding, Z. Wang, Y. Liu, Synthesis of ordered arrays of magnesium hydroxide nanoparticles via a simple method, Colloids Surf., A, 356 (2010) 28–31.

[41] C. Sun, X. Feng, Enhancing the performance of PVDF membranes by hydrophilic surface modification via amine treatment, Sep. Purif. Technol., 185 (2017) 94–102.

[42] L. Zhu, Y. Wang, F. Hu, H. Song, Structural and friction characteristics of g-C_3N_4/PVDF composites, Appl. Surf. Sci., 345 (2015) 349–354.

[43] J. Lv, G. Zhang, H. Zhang, C. Zhao, F. Yang, Improvement of antifouling performances for modified PVDF ultrafiltration membrane with hydrophilic cellulose nanocrystal, Appl. Surf. Sci., 440 (2018) 1091–1100.

[44] X. Zhao, N. Jia, L. Cheng, L. Liu, C. Gao, Dopamine-induced biomimetic mineralization for *in situ* developing antifouling hybrid membrane, J. Membr. Sci., 560 (2018) 47–57.

[45] C. Dong, C. Dai, S. Jiang, G. He, Application of $Mg(OH)_2$ nanoplatelets as pore former to prepare PVDF ultrafiltration membranes, J. Environ. Chem. Eng., 5 (2017) 877–883.